ILASS Americas, 21th Annual Conference on Liquid Atomization and Spray Systems, Orlando, FL, May 2008

Effect of Ambient Pressure and Impact Angle on Splashing Threshold during Droplet Impact

Jie Liu[1], Richard Jepsen[3], Sam S. Yoon[2] and Guillermo Aguilar[1,ψ]

[1]Department of Mechanical Engineering
University of California-Riverside
Riverside, CA 92507 USA
[2]Department of Mechanical Engineering
Korea University
Anamdong, 5-Ga, Sungbukgu, Seoul, 136-713, Korea
[3]Sandia National Laboratories
Albuquerque, NM 87185 USA

Abstract

While the threshold of splashing when liquid droplets impact against rigid solid surfaces is known to be related to the Weber number (*We*), the effect of ambient gas pressure (or density) and the impact angle have not been systematically studied. In this study, we examine the effects of droplet velocity, impact angle, and ambient gas pressure (or density) on the threshold of splashing. In our methodology, a FC-72 droplet of 1.7 mm in diameter is used, and the droplet velocity, impact angle, and ambient pressure are varied systematically. Then a semi-empirical and analytical correlation is developed based on experimental results. This correlation demonstrates that when the internal droplet pressure, which is caused by the change of momentum of the droplet during the impact process, is larger than the stress due to the surface tension, splashing occurs. Also, this correlation considers the reduction in the splashing as the droplet impact angle increases.

ψ Corresponding author: gaguilar@engr.ucr.edu

1. INTRODUCTION

One of the earliest studies of splashing after a liquid droplet impinges against a solid surface was carried by Worthington 100 years ago [1]. Droplet impact against solid and liquid surfaces have been widely used for materials processing, ink printing, spray cooling, and irrigation, although the physical mechanisms of splashing are still not completely explained. One of the most accepted explanations of the occurrence of splashing was offered by Engle [2] and states that the pressure variation inside the droplet during impact is the key factor that initiates splashing. Engle's theory [2] is proved by studies of droplet impact against a rigid surface at velocities over 100 m/s, which show that splashing is attributed to a pressure related shockwave caused by the "water hammer effect" at the beginning stage of droplet contact with the rigid solid surface [3-10]. Further studies show that splashing occurs as the momentum of the liquid droplet cannot convert into momentum of the liquid layer spreading along the impact surface after impact [11, 12]. This momentum conversion becomes more difficult when surface roughness is increased [13-15] or a vertical obstacle is added on the solid surface [16]. Consequently, the splashing is facilitated due to the pressure buildup at the front edge of the flow along the impact surface. Several studies have been carried on to qualitatively investigate the effect of impact velocity, droplet size [17, 18], surface temperature [19, 20] and properties of the liquid surface on droplet splashing [21-23], but the effect of ambient pressure and impact angle on splashing have not been considered yet. Recently, Xu *et al* found that as the ambient pressure drops below a certain value, splashing diminishes [24]. Jepsen *et al* [25] experimentally explained how the ambient pressure affected the splashing.

In this study, FC-72 and water droplets impact against a rigid solid dry surface at different inclination angles with ambient pressures ranging from 1 to 6 atm. Based on the experimental results, we develop an empirical model that uses the force balance between the droplet internal pressure and the droplet surface tension to predict the threshold of splashing.

2. METHODS

The liquids used in this study were water and C_6F_{14} (FC-72) Fluorinert, whose properties are shown in Table 1. FC-72 is normally used as an electronic cooling fluid. Its low surface tension property provides a wide range of values for the Weber number (*We)*. For this study, it was used as a surrogate of hydrocarbon fuels and cryogenic liquids. A precision micro-liter valve (Model 740V-SS, EFD Inc., East Providence, RI, USA) with stainless steel tips of various outer diameters was used to generate 1.7 mm diameter droplets. The distance from the nozzle tip to the impact surface was varied from 0.06 to 1.32 m to ensure impact velocities from 1 to 5 m/s. A smooth Plexiglas surface with less than 0.8 μm in roughness was mounted on a rotary stage (Model B5990TS, Velmex Inc., Bloomfield, NY, USA) at various impact angles ranging from 0^o to 60^o relative to the horizontal plane. The temperatures of the droplets and the Plexiglas were fixed at 298 K to maintain constant fluid properties and eliminate any variability due to evaporative cooling.

	H_2O	**FC-72**	**CH_3OH**
Density ρ (kg/m^3)	1000	1680	791
Surface tension σ *(mN/m)/Temp*	73	12.0	26
Viscosity μ (kg/m.s)	0.0009	0.00064	0.00058
Boiling point (^oC)	100	56	65

Table 1. Properties of the liquids

In this study, a controllable pressure chamber made of aluminum and equipped with two polycarbonate glasses for illumination and photography were used to carry out experiments at internal pressures ranging from 1 to 6 atm. Dry air of the same temperature as the surface and droplet temperature was used to pressurize the chamber. The images of the impact, spreading, and splashing were captured using a FastCam high-speed video camera at a rate of 2,000 frames per second. The high speed camera was fixed either at the same level as the impact surface to record the side view of the droplet impact or 30^o to the horizontal level to record the top view of the impact process.

3. EXPERIMENTAL RESULTS

3.1 Effect of the Weber Number (*We)*

Figure 1 [26] shows the effect of *We* on the impact dynamics. For *We* = 695 (left side), the water sheet spreads along the flat surface and no splash was observed. The liquid sheet that spreads along the flat surface for *We* = 695 was not observed for *We* = 1870. Instead, the edge of the liquid sheet was ejected at a certain angle from the horizontal plane at t = 0.11 ms. At t = 0.32 ms, a crown-shaped splash was clearly observed. At t = 0.85 ms, tiny water droplets were separated from the main crown structure of the liquid.

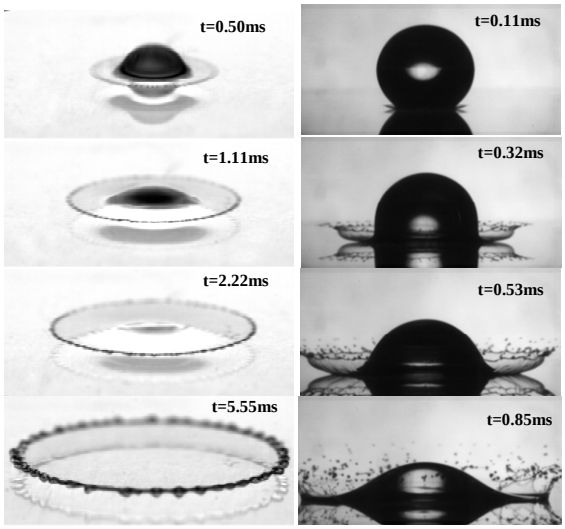

Figure 1. Effect of *We* on splashing. Left column: Water droplet with *We* = 695; and Right column: Methanol droplet with *We* = 1870 [26].

3.2 Effect of Ambient Pressure

Figure 2 shows the images of a FC-72 droplet impact against a flat surface for *We* = 1468 at different values of the ambient pressure ranging from 1 to 6 atm. At 1 atm, no splashing can be observed. As the pressure increased to 2 atm, mild splashing was observed at the advancing edge of the spreading layer at the surface. By further increasing the pressure to 4 atm, strong splashing was observed and the height of the splashed droplets at 4 atm was larger than that at 2 atm. At 6 atm, the splashing was so strong that it developed into disintegrated drops.

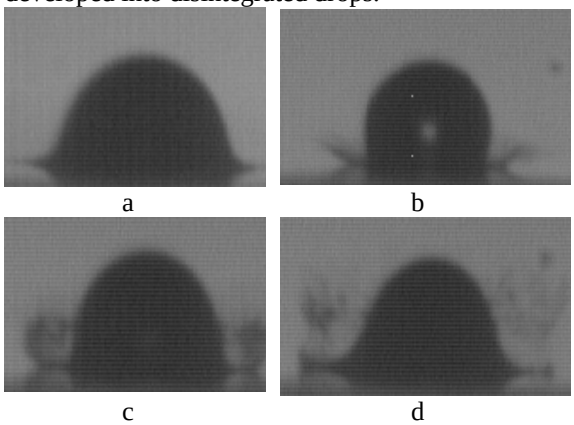

Figure 2. Effect of ambient pressure on splashing of a FC-72 droplet with *We* = 1468 and *Re* = 10708 on flat surface. Ambient pressure was (a) 1 atm; (b) 2 atm; (c) 4 atm; and (d) 6 atm.

Figure 3 shows the sequential images from a top view of a FC-72 droplet impact against a 45^o inclined surface for *We* = 970 at different values of ambient pressure: 1, 4 and 6 atm. At 1 atm, the edge of the spreading was smooth and no splashing or disintegrated liquid could be observed. As the pressure increased to 4 atm, weak splashing appeared only in the downhill direction. As the pressure further increased to 6 atm, splashing became prominent in the downhill direction. Though the ambient pressures were different, the shapes of the spreading after impact were similar; and the length of the spreading in the downhill direction was larger than that in uphill direction. Also, the length of the spreading layer in the longitudinal direction was larger than that in the latitude direction because of gravity.

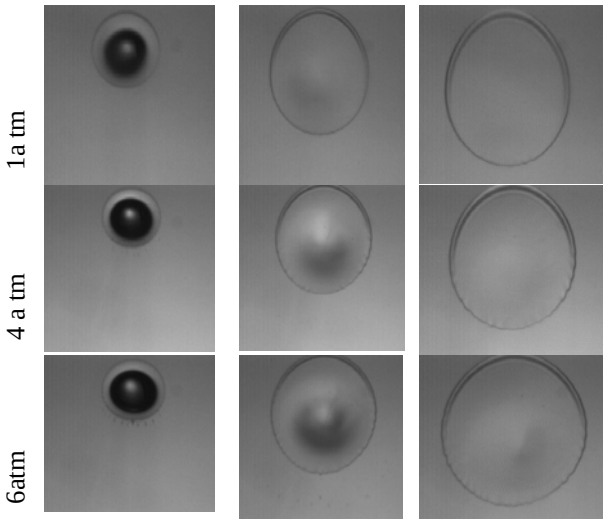

Figure 3. Effect of ambient pressure on splashing for a 45^o inclined surface. Ambient pressure: 1, 4 and 6 atm with FC-72 droplet with *We* = 970 and *Re* = 8700.

3.3 Effect of Impact Angle

In addition to the ambient pressure, the impact angle was another important parameter that affected the splashing. Figure 4 shows the impact of a FC-72 droplet onto an inclined Plexiglas surface at angles of 0, 15^o, 30^o and 45^o for *We* = 970 and gas pressure of 4 atm. For the flat surface, the splashing was almost symmetric. As the inclined angle increases to 15^o, the splashing became asymmetric and the splashing in downhill direction was stronger than that in uphill direction. With 30^o inclined angle, splashing could only be observed in the downhill direction and was much weaker than that with 15^o. With the 45^o inclined angle, the splashing almost disappeared completely.

Figure 5 shows the sequence of the top view image of droplet with *We* = 970 and *Re* = 8700 impacting against the surface with inclined angles of 15^o, 30^o, 45^o and 60^o at 4 atm. For the 15^o inclined surface, the splashing or instability was almost evenly distributed around the edges of the spreading

front edge. For the 30° inclined angle, the splashing still could be clearly observed only in the lower half of the spreading. For the 45° inclined angle, the splashing almost could not be observed. The splashing or instability totally disappeared with the 60° inclined angle.

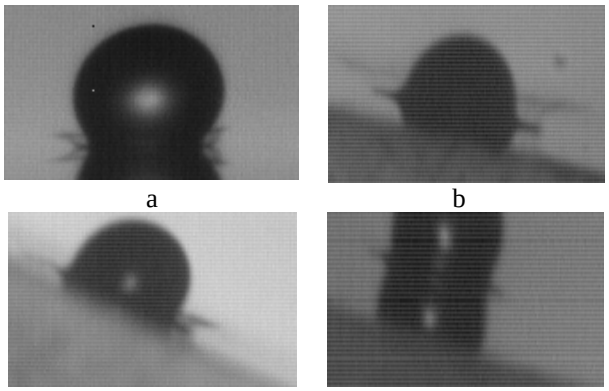

Figure 4. Effect of impact surface angle. (a) inclined angle 0°; (b) inclined angle 15°; (c) inclined angle 30°; (d) inclined angle 45° with FC-72 droplet with *We* = 970 and *Re* = 8700 at 4 atm.(side view)

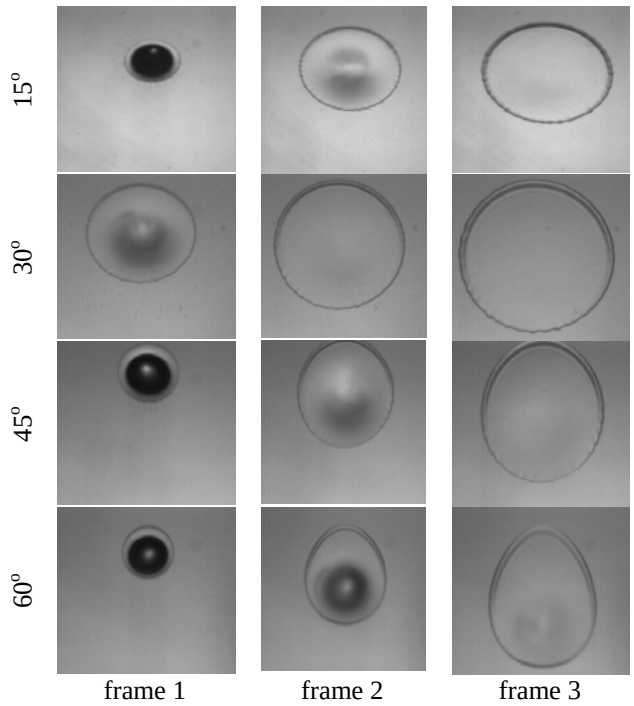

Figure 5. Effect of impact surface angle. (a) inclined angle 15°; (b) inclined angle 30°; (c) inclined angle 45°; (d) inclined angle 60° with FC-72 droplet with *We* = 970 and *Re* = 8700 at 4 atm.(side view)

4. ANALYSIS

Figure 1 shows that splashing occurred for a droplet moving at 3.5 m/s for a *We* of 1760, but did not occur for a droplet moving at *V*= 1.9 m/s or *We* = 562. Even though the spreading velocity increases with the increasing impact velocity, the relationship is not linearly proportional and eventually the dimensionless velocity *Vs/V* decreases with increasing impact velocity [25]. Thus, at low impact velocities, the droplet can convert its momentum onto a spreading flow along the impact surface, without splashing. As impact velocities increase beyond a critical *Vs/V* ratio, all the momentum from the impacting droplet cannot be transferred onto the spreading within the short time period of the impact, and splashing occurs. According to previous research, the pressure inside the droplet is generated during the process of impact or during the conversion of the momentum of the impacting droplet into the momentum of the liquid in the direction of flow along the impact surface [12]. Once the inside pressure becomes greater than the stress at the front of edge due to the surface tension, splashing occurs. The most recognized theory that explains how pressure is generated in the droplet during droplet impact is the "water hammer" effect [2], where

$$P = \rho V C_l \,. \qquad (1)$$

In the previous equation, C_l is the speed of sound in the liquid and ρ is the liquid density. In the water hammer effect, the liquid on the contact area is compressed and pressure is generated as the shockwave propagates in the liquid with the speed of sound. Once the front of the shockwave reaches the free surface of the liquid droplet, spreading or splashing is initiated. The water-hammer theorem concludes that the pressure due to the impact initiates splashing. However, previous research omitted the effect of ambient pressure, which has a major influence on the splashing, and only considered the cases in which the droplet velocity was over 100 m/s. Xu [27] modified Eq. 1, and the pressure due to the water hammer effect for low impact velocity was expressed as

$$P \sim \rho_g V_S C_g \,, \qquad (2)$$

where ρ_g is the gas density, V_S is the spreading velocity after droplet impact on a solid surface, and Cg is the speed of sound in the gas. Considering the ideal gas formulation, ρ_g can be written as

$$\rho_g = \frac{pM_m}{R_u T} \quad , \qquad (3)$$

where p is the ambient gas pressure, T is the gas temperature, M_m is the molecular weight of the gas, and R_u is the universal gas constant (8314 N m/kgmol K). The speed of sound in the gas is expressed as

$$C_g = \sqrt{\frac{nR_uT}{M_m}} \quad , \tag{4}$$

where n is the adiabatic constant for a compressible gas. The velocity of the spreading edge is

$$V_S = \sqrt{\frac{DV}{4t}} . \tag{5}$$

Thus, the pressure caused by the shock wave can be expressed as:

$$P \sim \rho_g C_g V_S = \frac{pM_m}{R_uT} \cdot \sqrt{\frac{nR_uT}{M_m}} \cdot \sqrt{\frac{DV}{4t}} \quad . \tag{6}$$

The stress caused by the surface tension can be expressed as:

$$\tau_{ST} = \sigma / h = \sigma / \sqrt{\nu t} \quad , \tag{7}$$

where σ is the surface tension, h is the thickness of the liquid layer and ν is the kinematic viscosity of the liquid. Thus, the splash occurs when the ratio of

$$P / \tau_{ST} \sim \sqrt{nM_m}\, p \cdot \sqrt{\frac{DV}{4R_uT}} \frac{\sqrt{\nu}}{\sigma} > S_{critical} . \tag{8}$$

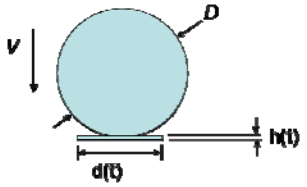

Figure 6. Sketch of the spreading after droplet impact onto rigid flat surface.

Until now, the most accepted explanation has been that splashing occurs once the momentum of the droplet cannot be converted into the momentum of liquid in the direction of flow along the surface [6]. Although the droplet impact is a dynamic and transient process, we simplified the impact analysis by assuming that the droplet impact was a pseudo-steady state process, as shown in Fig. 6, to illustrate the effects of droplet velocity and impact angle on the pressure variation inside the droplet. During this pseudo-steady state impact process, the momentum variation of the droplet at contact with the impact surface can be expressed as

$$\frac{dm\vec{V}_n}{dt} = \vec{F} = P\left(\pi r^2\right), \tag{9}$$

where $\vec{V}_n$ and P are the velocity and pressure of the droplet normal to the impact surface, respectively. r is the radius of the spreading layer defined as [28]

$$r(t) = R_m\left(1 - e^{-t/t_c}\right) \tag{10}$$

In equation (10), R_m is the maximum spreading radius that can be expressed as [29]

$$R_m = \frac{D}{2}\sqrt{\frac{We+12}{3(1-cos(\theta)) + 4\left(We/\sqrt{Re}\right)}} \quad , \tag{11}$$

t_c is the characteristic spreading time, which is given as the time from initial droplet contact to maximum spreading. This time can be approximated as *8D/3V* [30]. The thickness (h) of the spreading layer can be expressed [27] as

$$h = \sqrt{\frac{\mu t}{\rho}} \quad . \tag{12}$$

And the mass of the spreading layer can be expressed as

$$\pi\left(r(t)\right)^2 h(t)\rho \quad . \tag{13}$$

Inserting Eqs. 10-13 into the left hand side of Eq. 9 and solving for P yields

$$P = \left|\vec{V}_n\right|\sqrt{\rho\mu}\left(\frac{2e^{-t/t_c}\sqrt{t}}{t_c\left(1-e^{-t/t_c}\right)} + \frac{1}{2\sqrt{t}}\right) . \tag{14}$$

where $\left|\vec{V}_n\right| = V\cos(\alpha)$, and α is the inclined impact surface angle in this study. The ratio of P to the shear stress caused by the surface tension (τ_{ST}) Eq. 7 is then expressed as

$$P / \tau_{ST} = P/\left(\sigma/\sqrt{\nu t}\right) \approx 2.5\frac{\left|\vec{V}_n\right|\mu}{\sigma} = 2.5\frac{We}{\mathrm{Re}} = 2.5Ca_n \tag{15}$$

where $We = \frac{\rho DV^2}{\sigma}$, $Re = \frac{\rho DV}{\mu}$ and $C_a = \frac{We}{Re}$.

Figures 2 and 3 show that the ambient pressure also affects the threshold for splashing. To predict the threshold of splashing ($S_{critical}$), we propose the following power law correlation, which must yield a value larger than 0.45 according to previous studies [27]:

$$S_{critical} \sim c_1(Ca_n)^{c_2}\left(\frac{p}{P_o}\right)^{c_3} > 0.45 \ , \tag{16}$$

where p is the gas pressure and P_o is equal to the atmospheric pressure. The coefficients c_1, c_2 and c_3 can be obtained from experimental results and Eq. 16 may be re-arranged by dividing 0.45 on both sides to yield

$$2.84(Ca_n)^{0.5}\left(\frac{p}{P_o}\right)^{0.42} > 1\,, \qquad (17)$$

where Ca is the capillary number defined as We/Re.

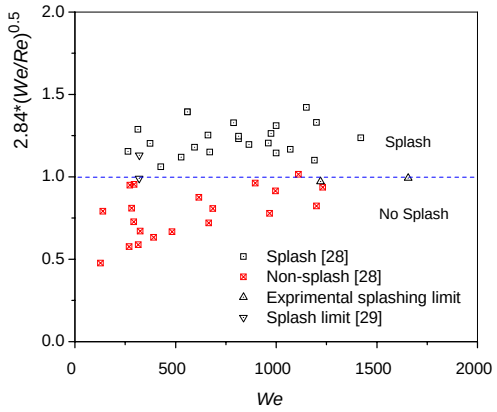

Figure 7. Model predicted splashing limit vs. experimental results.

Figure 7 shows proof that as long as the correlation given by Eq. 17 is greater than 1, splashing events can be differentiated from those without splashing for a range of We ~ 100 to 1600. Vander Wal et al. used liquid droplets of a fixed size moving at various velocities to determine the splashing threshold. In Fig 7, the Vander Wal et al's [28] and Rioboo et al's [29] experimental data distribute evenly around the splash threshold given by Eq. 17.

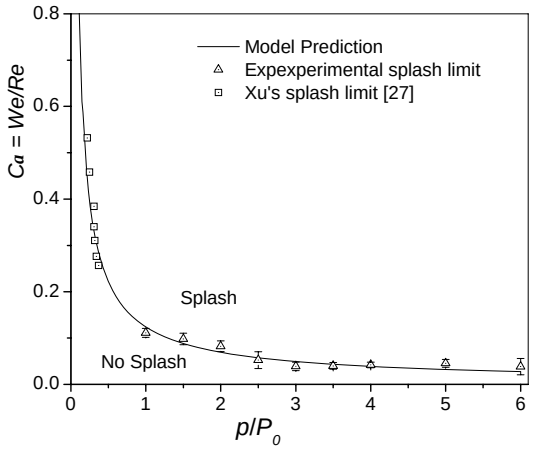

Figure 8. Model predicted splashing limit vs. experimental results.

Figure 8 shows another representation of the predictions of the splash threshold given by Eq. 17 but now as a function of the gas pressure p, normalized by the atmospheric pressure P_o. This curve shows that, for sub-atmospheric pressures (p/P_0 <1), the Ca number for the splashing threshold increases dramatically for lower pressures but it reaches a near constant value as the pressure increases above atmospheric. For sub-atmospheric pressures, Xu's [27] experimental data also show strong agreement with the correlation proposed by Eq. 17.

Eq. 17 also shows that the droplet velocity normal to the impact surface plays an important role in determining the splashing threshold. As the impact angle increases, the droplet velocity normal to the impact surface is reduced, and both our experimental results and prediction by Eq. 17 show that the occurrence of splashing becomes less likely.

5. CONCLUSIONS

Both experimental results and model prediction show that as the ambient pressure increases, the splashing increases correspondingly. Also, the splashing reduces as the velocity normal to the impact surface reduces with increasing impact angle.

Nomenclature

C_a	capillary number (We/Re or $V\mu/\sigma$)
C_g	sound speed in ambient gas [m/s]
C_l	sound speed in liquid [m/s]
$\vec{F}$	force [N]
k	wave number
h	thickness of flatten cryogen at maximum spread diameter [m]
m	mass [kg]
n	gas constant
M_m	molecular weight of the gas [g/mol]
$\vec{V}_n$	impact velocity in normal direction to the impact surface [m/s]
V_{rel}	relative velocity [m/s]
p	ambient gas pressure [Pa]
P_o	atmospheric pressure [1atm]
P	pressure inside droplet [Pa]
r	radius of cryogen spread [m]
R_m	maximum spread radius [m]
Re	Reynolds number ($\rho VD/\mu$)
Ru	universal gas constant [8314 N m/kgmol K]
t	time [s]
t_c	critical time [s]
T	temperature [^{o}C]
T_{sat}	saturation temperature of cryogen at 1 atm [^{o}C]
V	droplet velocity [m/s]
V_{rel}	relative velocity [m/s]

V_s	spreading velocity [m/s]
W_{Diss}	energy dissipated during cryogen spread [m s]
We	Weber number ($D\rho V^2/\sigma$)

Greek symbol

α	impact angle or inclined angle of impact surface
μ	dynamic viscosity [kg/s m]
ν	kinematic viscosity [m^2/s]
ω	interface growth rate [m/s^2]
θ	static wetting angle [^{o}]
ρ	liquid density [kg/m^3]
ρ_g	ambient gas density [kg/m^3]
σ	surface tension [N/m]
τ_{ST}	shear stress caused by surface tension [N/m^2]

Reference

1. Worthington, A., *On the froms assumed by drops of liquids falling vertically on a horizontal plate.* Proc. R. Soc. London, 1876. **25**: p. 261-271.
2. Engel, O.G., *Waterdrop Collisions with Solid Surfaces.* Journal of Research of the National Bureau of Standards, 1955. **54**(5): p. 281-298.
3. Bowden, F.P. and Field, J.E., *Brittle Fracture of Solids by Liquid Impact by Solid Impact + by Shock.* Proceedings of the Royal Society of London Series a-Mathematical and Physical Sciences, 1964. **282**(139): p. 331-&.
4. Hobbs, P.V. and Osheroff, T., *Splashing of Drops on Shallow Liquids.* Science, 1967. **158**(3805): p. 1184-&.
5. Hobbs, P.V. and Kezweeny, A.J., *Splashing of a Water Drop.* Science, 1967. **155**(3766): p. 1112-&.
6. Levin, Z. and Hobbs, P.V., *Charge Separation Due to Splashing of Water Drops.* Bulletin of the American Meteorological Society, 1970. **51**(6): p. 577-&.
7. Levin, Z. and Hobbs, P.V., *Splashing of Water Drops on Solid and Wetted Surfaces - Hydrodynamics and Charge Separation.* Philosophical Transactions of the Royal Society of London Series a-Mathematical and Physical Sciences, 1971. **269**(1200): p. 555-&.
8. Lesser, M.B., *Analytic Solutions of Liquid-Drop Impact Problems.* Proceedings of the Royal Society of London Series a-Mathematical Physical and Engineering Sciences, 1981. **377**(1770): p. 289-308.
9. Lesser, M.B. and Field, J.E., *The Impact of Compressible Liquids.* Annual Review of Fluid Mechanics, 1983. **15**: p. 97-122.
10. Field, J.E., et al., *Studies of Two-Dimensional Liquid-Wedge Impact and Their Relevance to Liquid-Drop Impact Problems.* Proceedings of the Royal Society of London Series a-Mathematical Physical and Engineering Sciences, 1985. **401**(1821): p. 225-&.
11. Stow, C.D. and Hadfield, M.G., *An Experimental Investigation of Fluid-Flow Resulting from the Impact of a Water Drop with an Unyielding Dry Surface.* Proceedings of the Royal Society of London Series a-Mathematical Physical and Engineering Sciences, 1981. **373**(1755): p. 419-441.
12. Harlow, F.H. and Shannon, J.P., *Splash of a Liquid Drop.* Journal of Applied Physics, 1967. **38**(10): p. 3855-&.
13. Range, K. and Feuillebois, F., *Splashing of a drop on a rough surface.* High Temperature Material Processes, 1998. **2**(2): p. 287-300.
14. Range, K. and Feuillebois, F., *Influence of surface roughness on liquid drop impact.* Journal of Colloid and Interface Science, 1998. **203**(1): p. 16-30.
15. Field, J.E., *ELSI conference: invited lecture - Liquid impact: theory, experiment, applications.* Wear, 1999. **235**: p. 1-12.
16. Josserand, C., et al., *Droplet impact on a dry surface: triggering the splash with a small obstacle.* Journal of Fluid Mechanics, 2005. **524**: p. 47-56.
17. Bussmann, M., et al., *Modeling the splash of a droplet impacting a solid surface.* Physics of Fluids, 2000. **12**(12): p. 3121-3132.
18. Rieber, M. and Frohn, A., *A numerical study on the mechanism of splashing.* International Journal of Heat and Fluid Flow, 1999. **20**(5): p. 455-461.
19. Pasandideh-Fard, M., et al., *A three-dimensional model of droplet impact and solidification.* International Journal of Heat and Mass Transfer, 2002. **45**(11): p. 2229-2242.
20. Francois, M. and Shyy, W., *Computations of drop dynamics with the immersed boundary method, part 2: Drop impact and heat transfer.* Numerical Heat Transfer Part B-Fundamentals, 2003. **44**(2): p. 119-143.
21. Weiss, D.A. and Yarin, A.L., *Single drop impact onto liquid films: neck distortion, jetting, tiny bubble entrainment, and crown*

formation. Journal of Fluid Mechanics, 1999. **385**: p. 229-254.
22. Josserand, C. and Zaleski, S., *Droplet splashing on a thin liquid film.* Physics of Fluids, 2003. **15**(6): p. 1650-1657.
23. Yarin, A.L. and Weiss, D.A., *Impact of Drops on Solid-Surfaces - Self-Similar Capillary Waves, and Splashing as a New-Type of Kinematic Discontinuity.* Journal of Fluid Mechanics, 1995. **283**: p. 141-173.
24. Xu, L., *Liquid drop splashing on smooth, rough, and textured surfaces.* Physical Review E, 2007. **75**(5): p.505-516.
25. Jepsen, R.A., et al., *Effects of air on splashing during a large droplet impact: Experimental and numerical investigations.* Atomization and Sprays, 2006. **16**(8): p. 981-996.
26. Yoon, S.S. and DesJardin, P.E., *Modelling spray impingement using linear stability theories for droplet shattering.* International Journal for Numerical Methods in Fluids, 2006. **50**(4): p. 469-489.
27. Xu, L., et al., *Drop splashing on a dry smooth surface.* Physical Review Letters, 2005. **94**(18): p. 26-28.
28. Vander Wal, R.L., et al., *The splash/non-splash boundary upon a dry surface and thin fluid film.* Experiments in Fluids, 2006. **40**(1): p. 53-59.
29. Rioboo, R., et al., *Experimental evidence of liquid drop break-up in complete wetting experiments.* Journal of Materials Science, 2006. **41**(16): p. 5068-5080.